

Developmentally interdependent stretcher-compressor relationship between the embryonic brain and the surrounding scalp in the preosteogenic head

Koichiro Tsujikawa¹ | Kanako Saito^{1,2} | Arata Nagasaka³ | Takaki Miyata¹ 

¹Department of Anatomy and Cell Biology, Nagoya University Graduate School of Medicine, Nagoya, Japan

²Department of Physiology, Fujita Health University, Toyoake, Japan

³Division of Anatomy, Meikai University School of Dentistry, Sakado, Japan

Correspondence

Takaki Miyata, Department of Anatomy and Cell Biology, Nagoya University Graduate School of Medicine, 65 Tsurumai, Showa, Nagoya 466-8550, Japan.
Email: tmiyata@med.nagoya-u.ac.jp

Funding information

Japan Society for the Promotion of Science, Grant/Award Numbers: 21H02656, 21H00363, 19K22683, 16H02457

Abstract

Background: How developing brains mechanically interact with the surrounding embryonic scalp layers (ie, epidermal and mesenchymal) in the preosteogenic head remains unknown. Between embryonic day (E) 11 and E13 in mice, before ossification starts in the skull vault, the angle between the pons and the medulla decreases, raising the possibility that when the elastic scalp is directly pushed outward by the growing brain and thus stretched, it recoils inward in response, thereby confining and folding the brain.

Results: Stress-release tests showed that the E11-13 scalp recoiled and that the in vivo prestretch prerequisite for this recoil was physically dependent on the brain (pressurization at 77-93 Pa) and on actomyosin and elastin within the scalp. In scalp-removed heads, brainstem folding was reduced, and the spreading of ink from the lateral ventricle to the spinal cord that occurred in scalp-intact embryos (with >5 μ L injection) was lost, suggesting roles of the embryonic scalp in brain morphogenesis and cerebrospinal fluid homeostasis. Under nonstretched conditions, scalp cell proliferation declined, while the restretching of the shrunken scalp rescued scalp cell proliferation.

Conclusions: In the embryonic mouse head before ossification, a stretcher-compressor relationship elastically develops between the brain and the scalp, underlying their mechanically interdependent development.

KEYWORDS

cerebrospinal fluid, epidermis, mesenchyme, morphogenesis, mouse, tension

1 | INTRODUCTION

Intertissue forces play important roles in a variety of morphogenetic events.¹ For example, mechanical influences

on blastocysts from the trophectoderm or those on cylinder-shaped embryos from the uterine wall facilitate embryogenesis.^{2,3} Additionally, the development of tubular structures, such as the gut, bronchi, and oviducts, is driven by mechanical relationships between the inner and outer layers, enabling villification, branching, or fold

Koichiro Tsujikawa and Kanako Saito contributed equally to this study.

This is an open access article under the terms of the [Creative Commons Attribution-NonCommercial-NoDerivs](https://creativecommons.org/licenses/by-nc-nd/4.0/) License, which permits use and distribution in any medium, provided the original work is properly cited, the use is non-commercial and no modifications or adaptations are made.

© 2022 The Authors. *Developmental Dynamics* published by Wiley Periodicals LLC on behalf of American Association for Anatomy.

pattern formation on the inner epithelial sheet.⁴⁻⁸ In these examples, constraint or confinement by an external or superficial layer is a key mechanical factor that enables the deeper structure (under physiological compression) to continue normal development.^{9,10} Through “morphomechanical” approaches combining experimental and computational data, Taber et al^{11,12} found that invagination during chicken optic cup formation is driven by external confining factors such as the ectoderm and the extracellular matrix.

In the developing vertebrate brain, intramural cellular and tissue mechanics have recently been explored.^{13,14} The possible biomechanical influence of growing brains on the formation of the surrounding skull or cranial vaults (in events such as osteoblast proliferation and ossification, by stretching the cells undergoing these events) has been discussed.¹⁵ Conversely, it has been proposed that the ossified skull (as a hard capsule) regulates brain morphology, including the gyrification of the cerebral cortex,¹⁶ although experimental and mathematical studies have suggested that gyrification may physically proceed through mechanisms intrinsic to the brain.¹⁷⁻¹⁹ These previous studies on possible brain-skull mechanical relationships in mammals have mainly focused on stages after ossification/mineralization has occurred. In the earlier (ie, preosteogenic) stage, studies performed in chicken embryos suggested a model in which the emergence of the flexure in the early neural tube (a phenomenon in which the anterior-most procerephalon bends ventrally) might be explained by a possible physical constraint imposed by the ventrally underlying notochord or foregut, which are structures that are less extended anteriorly than the procerephalon,^{20,21}

and this model was recently supported by a mechano-mathematical simulation analysis.²² Fias et al²³ suggested that the head mesenchyme superficial/lateral to the brain vesicles was under tension along the anterior-posterior axis in embryonic day 2 (E2) chick embryos, but it is proposed that the conversion of a hollow tube into the brain vesicles or rhombomeres is driven mainly by brain-intrinsic mechanical mechanisms.^{22,23} Thus, the mechanical properties of the mesenchymal and epidermal tissues that externally/dorsally cover the brain at the preosteogenic stage and how the embryonic brain mechanically interacts with the scalp remain poorly understood across all vertebrate groups, especially mammals.

A survey of sagittal sections examining how brain vesicles grow under space limitation within the heads of mouse embryos (Figure 1) showed that the angle between the pons and the medulla dramatically decreases between E11 and E13, thereby narrowing the fourth ventricle. We accordingly hypothesized that the dorsal “scalp” (herein designated on the basis of gross anatomy but histologically consisting of an epidermal layer and the underlying mesenchyme) might play a role in the confinement of the growing brain, inducing “brainstem folding” to decrease the pons-medulla angle. To investigate this possibility, we sought to examine (a) the histological and mechanical properties of the scalp (whether a tensile force exists in the in vivo scalp that explains its possible inward compression/confinement of the brain and, if so, the mechanisms by which such a force is generated in the scalp) and (b) brain responses upon the removal of the scalp (whether the brain recoils outward from a normal in vivo position when released from hypothetical constraint by

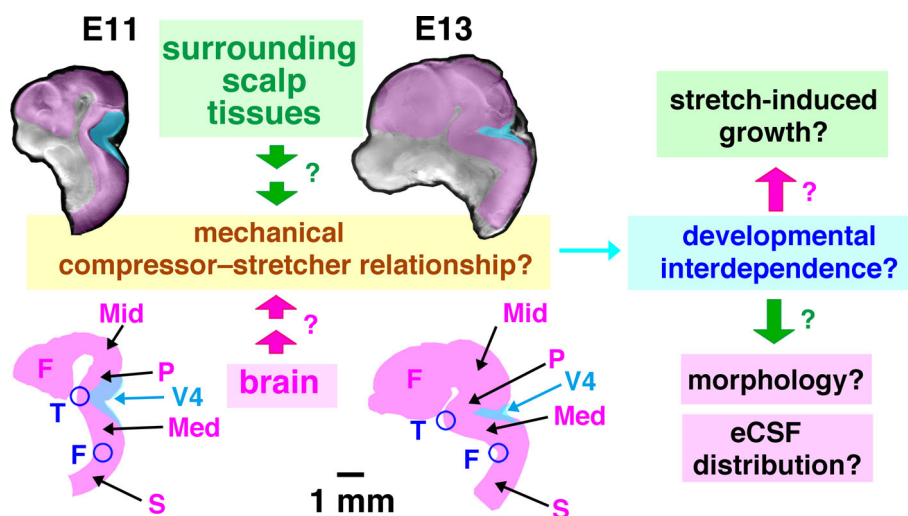


FIGURE 1 Hypothesis and questions: possible brain-scalp mechanical interactions during the E11-E13 period. Photomicrographs of the right half of the head are schematically highlighted (magenta, brain; blue, fourth ventricle). Between E11 and E13, the forebrain (F) and midbrain (Mid) vesicles expanded, the pons (P)-medulla (Med) angle decreased, and the fourth ventricle (V4) narrowed, raising the possibility that the brain pushed and stretched the overlying scalp and that the scalp, in return, compressed and constricted the brain. eCSF, embryonic cerebrospinal fluid; F, cervical flexure; S, cervical spinal cord; T, trigeminal root

the scalp). The mesenchymal element of the calvarial (ie, dorsally brain-covering) connective tissues during this E11-E13 period cannot be stained with Alizarin red or alkaline phosphatase at this time and is therefore known to be preosteogenic.²⁴⁻²⁸ Inspired by an example from the cardiovascular system in which the lower leg muscles contract and push the underlying veins to allow them to passively return blood to the heart,²⁹ we further asked whether the early embryonic scalp plays a constricting role similar to a leg muscle, perhaps contributing to normal embryonic cerebrospinal fluid distribution. Since the mesenchymal layer of the scalp and the adjacent overlying epidermal layer both tangentially expand as the brain grows outward, we also sought to investigate whether possible mechanical influences from the expansively growing brain promote the development of the scalp, especially the proliferation of epidermal and mesenchymal cells. To address these interrelated questions (Figure 1) about the potential biological significance of the mechanical interactions between the developing brain and the surrounding scalp in the preosteogenic embryonic mouse head, we performed a series of morphological, pharmacological, and mechanical examinations.

2 | RESULTS

2.1 | Immunohistochemical characterization of the calvarial epidermal and mesenchymal tissues during the E11-E13 period

To molecularly characterize the early embryonic mouse scalp to address questions regarding its mechanical

properties, we first subjected coronal sections of the heads of E12 embryos to immunohistochemistry using the antibodies listed in Figure 2. Low-magnification observations showed superficial immunoreactivity for alpha smooth muscle actin (α SMA), which has been suggested to function in cells playing force-generating and/or constricting roles,^{5,6,30,31} this immunoreactivity was continuously strong throughout the dorsal (calvarial) side of the head but not ventrally toward the face, producing a staining pattern similar to a cap (Figure 2A). High-power views of the dorsal scalp (Figure 2B) revealed that the most superficial layer was positive for cytokeratin 10 (CK10); therefore, this layer was identified as the epidermis. In a deeper zone, abundant immunoreactivity for α SMA with a fiber-like pattern was found, and most cell nuclei were positive for Runx2, indicative of a mesenchymal (dermal) nature.³² Collagen 4 (COL4), elastin, and phosphorylated myosin light chain (pMLC) were detected in both the epidermal and mesenchymal layers. Capillaries beneath the α SMA⁺ layer (and along/on the meninges) were also positive for COL4 and pMLC.

2.2 | The E11-E13 scalp is passively stretched and under tension

For execution of possible constricting or confining action against the brain as hypothesized (Figure 1), the scalp/calvarial tissue may have to show contractility and/or elasticity in situ. If such mechanical confrontation with the growing brain occurs, the scalp/calvarial tissue should be under tension. To investigate this possibility, microsurgical tests aimed at releasing residual tissue stresses were performed on freshly isolated embryos.

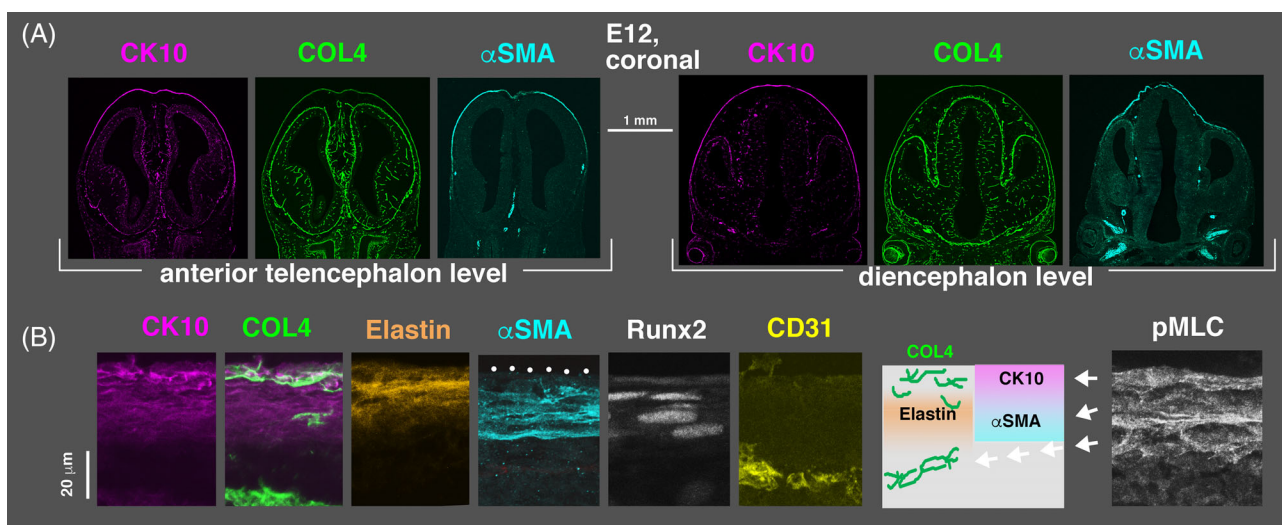


FIGURE 2 Immunohistochemical characterization of E12 scalp layers. (A) Low-power micrographs of coronal sections immunostained with anti-cytokeratin 10 (CX10), anti-collagen 4 (COL4), and anti-alpha smooth muscle actin (α SMA). (B) Magnified images of the dorsal scalp showing differential or overlapping staining patterns of CX10, COL4, elastin, and α SMA (schematically illustrated) as well as Runx2, CD31, and phosphorylated myosin light chain (pMLC)

When a small incision was made to the scalp along the anterior-posterior (AP) axis of the head (both the epidermal and mesenchymal layers were cut, but the underlying meninges were kept intact), the cut edges of the scalp immediately separated along the dorsoventral (DV) axis of the head, and the wound continued to separate for 30 min ($n = 2/2$ at E11; $n = 5/5$ at E12; $n = 3/3$ at E13)

(Figure 3A-C). In contrast, incisions made along the axial (body trunk) structures did not result in wide wound opening along the DV axis (Figure 3C). A DV incision in the scalp resulted in a similarly wide wound along the AP axis ($n = 2/2$) (data not shown). To determine whether this wound-opening response in the scalp truly reflected a physiological mechanism, rather than

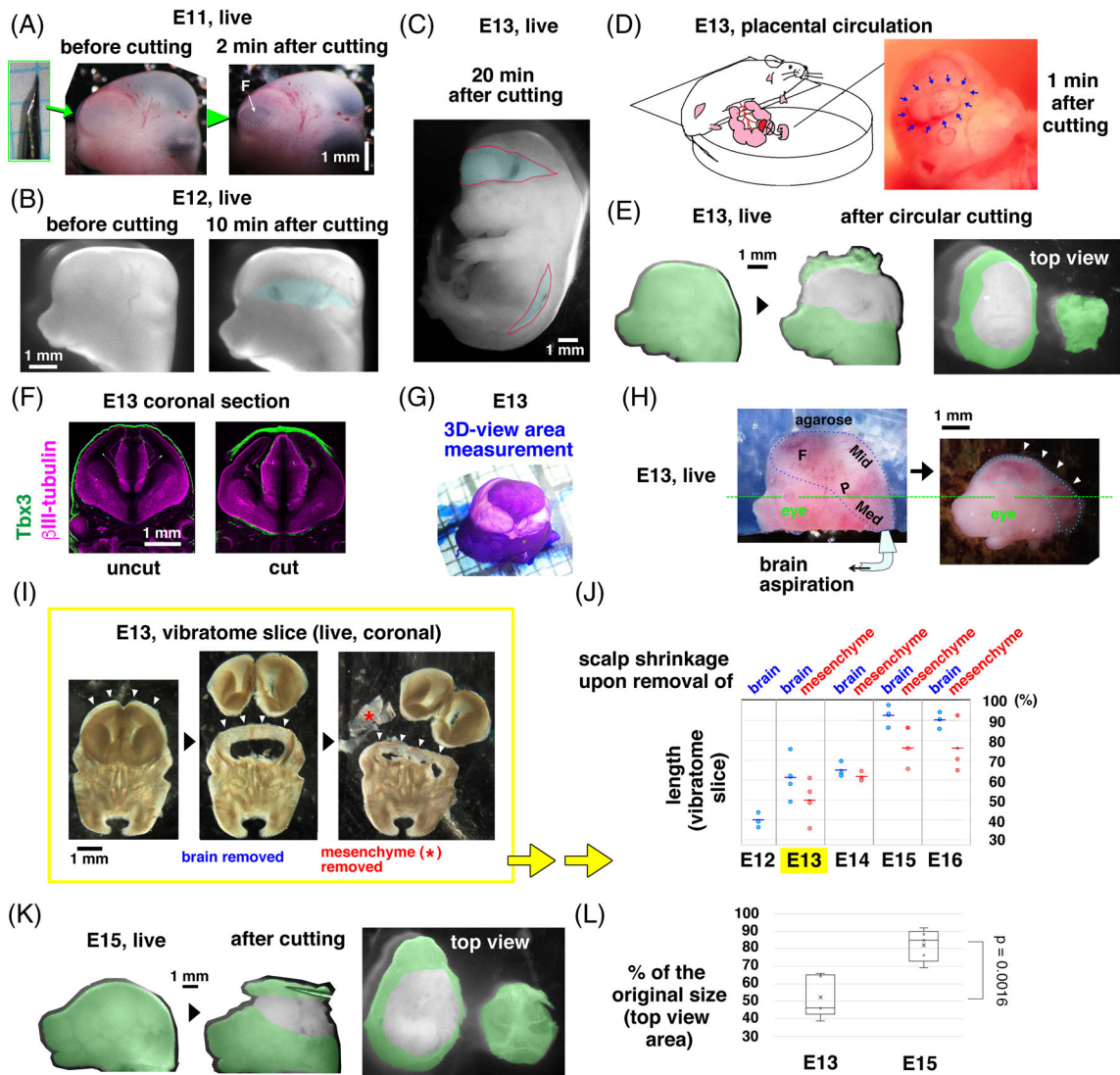


FIGURE 3 Stress-releasing tests reveal passive stretching and tension in the early embryonic scalp. (A) A horizontal incision made in the forebrain (F)-covering scalp of an E11 embryo immediately resulted in a wound. (B) Incision of the scalp of an E12 embryo followed by wound opening. (C) An E13 embryo subjected to an incision in the scalp over the brain and another incision near the spinal cord. (D) Incision in an E13 embryo with a beating heart that was connected to the anesthetized mother mouse. The incision produced an immediate wound-opening response. (E) Circular incision and subsequent shrinkage of the scalp at E13. (F) Coronal sections of control and scalp-shrunk heads immunostained for the epidermal marker Tbx3 and the neuronal marker βIII-tubulin. (G) A circularly incised E13 head stained with toluidine blue for 3D area measurement using Zephyr (see also Movie S1). (H) An E13 head freshly mounted in a block of low-melting-temperature agarose (left), from which the brain (F, forebrain; Mid, midbrain; P, pons; Med, medulla) was subsequently aspirated (right) until the scalp collapsed (arrowhead). (I) Removal of the brain (cerebral hemisphere) and mesenchyme from a vibratome slice of a head at E13 (see also Movie S2). (J) Graph summarizing stage-dependent changes in the degree of scalp shortening upon the removal of the brain as well as the mesenchyme (when applicable) from vibratome slices of the head. (K) An E15 head subjected to circular scalp incision. (L) Graph comparing the shrinkage of the circularly excised scalp between E13 and E15

resulting from embryo isolation and incubation in culture dishes, we made incisions in E13 embryos with beating hearts that were connected via the normal umbilical circulation to their anesthetized mother mice and found that the wound opening was reproduced ($n = 3/3$) (Figure 3D). To further quantify the degree of shrinkage (ie, the recoil from a prestretched state) of the E13 scalp, a circular incision was made, and measurements were performed from a top view (Figure 3E), coronal section view (Figure 3F), or 3D view (Figure 3G, Movie S1). Quantitatively, it was shown that when the scalp was disconnected from the skin of the face, it shrunk centripetally to $52 \pm 11\%$ (mean \pm SD, $n = 5$) (top-view analysis) of the original size/area by 20 min after the incision was made and shrunk further to $25 \pm 5\%$ ($n = 3$) (3D area measurement by Zephyr) of the original size/area by 40 min. Compared to the Zephyr-based 3D measurement (Figure 3G, Movie S1), the top-view measurement may have underestimated the shrinkage of the excised scalp because the area associated with a dome-like morphology may have been flat projected and interpreted to be narrower.

As another approach for testing whether the abovementioned brain-scalp mechanical confrontation occurred, we aspirated the brains from E13 heads (Figure 3H) and found that the dorsal scalp shrunk with kinetics and a magnitude similar to those of the circularly incised scalp (Figure 3E).

Further analysis of scalp shrinkage upon brain removal using coronal vibratome slices of the head (Figure 3I, Movie S2) showed stage dependence that was much weaker at E15-E16 than at E12-E14 (Figure 3J). When we also removed mesenchymal tissues, which gradually thickened and stiffened between E13 and E15 (probably reflecting differentiation toward osteogenesis^{25,26}), the shrinkage of the remaining scalp (almost purely epidermis) was facilitated overall, especially at E15 and E16 (though it was still weaker than at E12 or E13). A top-view comparison of scalp shrinkage between E15 (Figure 3K) and E13 (Figure 3E) showed that the recoil activity of the scalp was significantly greater at E13 ($52 \pm 11\%$ [mean \pm SD], $n = 5$) than at E15 ($82 \pm 8\%$, $n = 5$) ($P = .0016$, Welch's test) (Figure 3L). These results suggest that the E11-E13 period can be characterized as a stage when the scalp exhibits remarkable tissue-level responsiveness to recoil when released and that the in vivo prestretch prerequisite for this recoil depends on the existence of the brain.

Actomyosin inhibition reduces scalp shrinkage, while calyculin A-mediated excessive contraction of scalp cells causes buckling of the brain wall.

To determine whether the prestretched in vivo condition of the scalp, as evidenced by recoil in response to stress-releasing tests and mediated by the brain

(Figure 3), could also be explained by the autonomous contractility of the scalp, given that the scalp was positive for pMLC (Figure 2B), we pharmacologically inhibited actomyosin (Figure 4A,B). The shrinkage of the excised E12 scalp was significantly weaker when the scalp was exposed to blebbistatin (myosin II inhibitor) (shrinkage to $67 \pm 6\%$ of the original size [$n = 7$], $P = .018$ [Welch's test]) or Y27632 (rho kinase inhibitor) ($70 \pm 6\%$ [$n = 7$], $P = .007$) than in the control (DMSO) group ($55 \pm 12\%$, $n = 7$).

To further ask whether the hypothetical scalp-brain mechanical confrontation (presumably balanced in vivo) is based on optimized myosin-mediated contractility of the scalp, we sought to artificially increase scalp contractility via the overactivation of actomyosin. To this end, we took advantage of calyculin A, a phosphatase inhibitor that induces the contraction of MLC- or α SMA-expressing cells.^{33,34} When separate cultures of epidermal or mesenchymal cells spread flat on the dish surface were exposed to calyculin A, morphological changes (ie, shortening or rounding) consistent with contraction were observed in each culture (Figure 4C, D).

We then treated E12 heads with calyculin A ($1 \mu\text{M}$, 60 min) and, upon coronal sectional inspection, found that pMLC immunoreactivity was increased in scalp specimens with spot-like rather than normal fibrous staining patterns and that the cerebral walls were buckled and showed multiple abnormal convexities toward the ventricle ($n = 4/4$) (Figure 5A). In these calyculin A-treated heads, the brain showed no increase in pMLC immunoreactivity throughout the wall, including its apical surface, whose contraction has previously been shown to account for curvatures observed during morphogenesis of the brain vesicles and rhombomeres,^{22,23} suggesting that a direct effect of calyculin A on the brain across/beyond the scalp layers was unlikely or minimal in our experiments, if present at all. Similar buckling was observed in the dorsal midbrain wall ($n = 9/9$ sagittally sectioned heads) (Figure 5B). These results suggest that an optimized level of contractility dependent on actomyosin in vivo may be a major force-generating factor that drives the tangential narrowing of the scalp.

2.3 | The embryonic scalp also responds to elastase but not to collagenase

To examine the possible contribution of extracellular matrix proteins to the tangential narrowing behavior of the E11-E13 scalp, we also treated excised E12 scalp specimens with elastase or collagenase. Shrinkage was significantly weaker than under the control conditions (shrinkage to $55 \pm 12\%$ of the original size, $n = 7$) when the scalp was exposed to elastase ($66 \pm 9\%$ [$n = 10$],

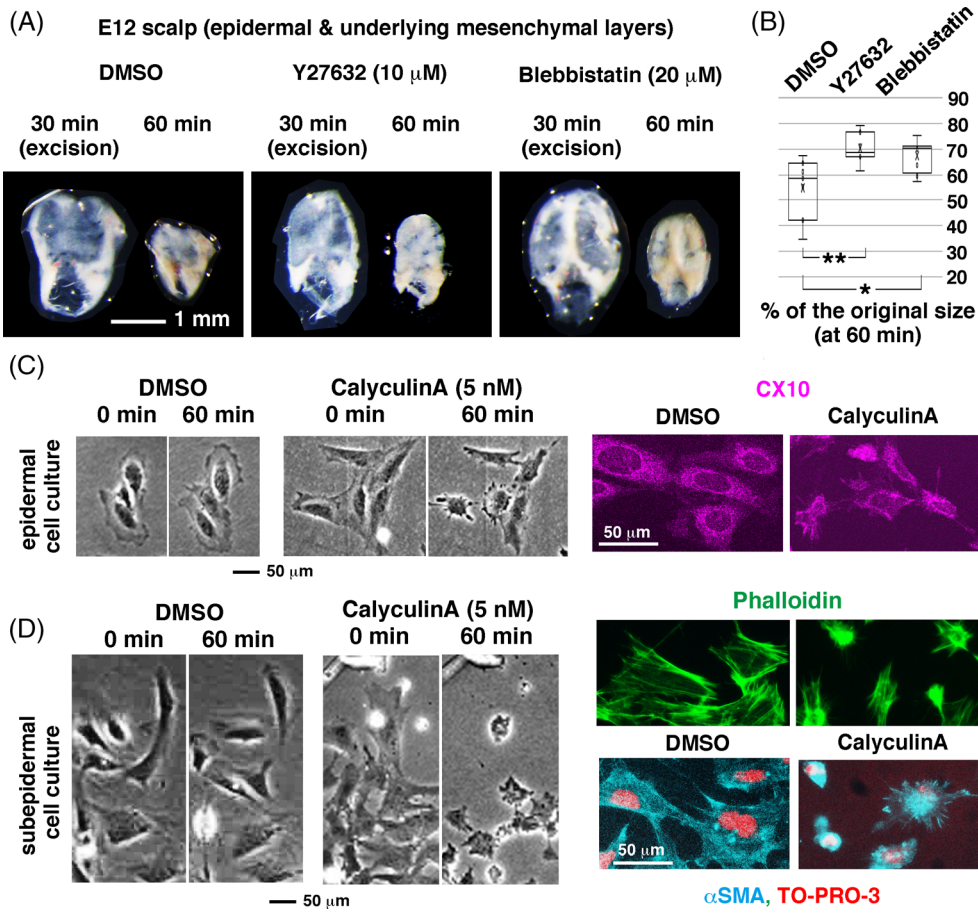


FIGURE 4 Pharmacological assessment of contractility in cultured scalp cells. (A) Top views of circularly excised scalps under DMSO, Y27632, or blebbistatin treatment. (B) Graph comparing the shrinkage of the circularly excised scalp among the control (DMSO), Y27632, and blebbistatin groups. * $P = .018$. ** $P = .007$. (C) Epidermal cells harvested from an E13 scalp and grown for 12 h shrank in response to calyculin A (subsequently confirmed to be of epidermal nature by CX10 immunoreactivity). (D) Cells from the E13 subepidermal layer cultured for 12 h also shrank in response to calyculin A (subsequently shown to be positive for α SMA)

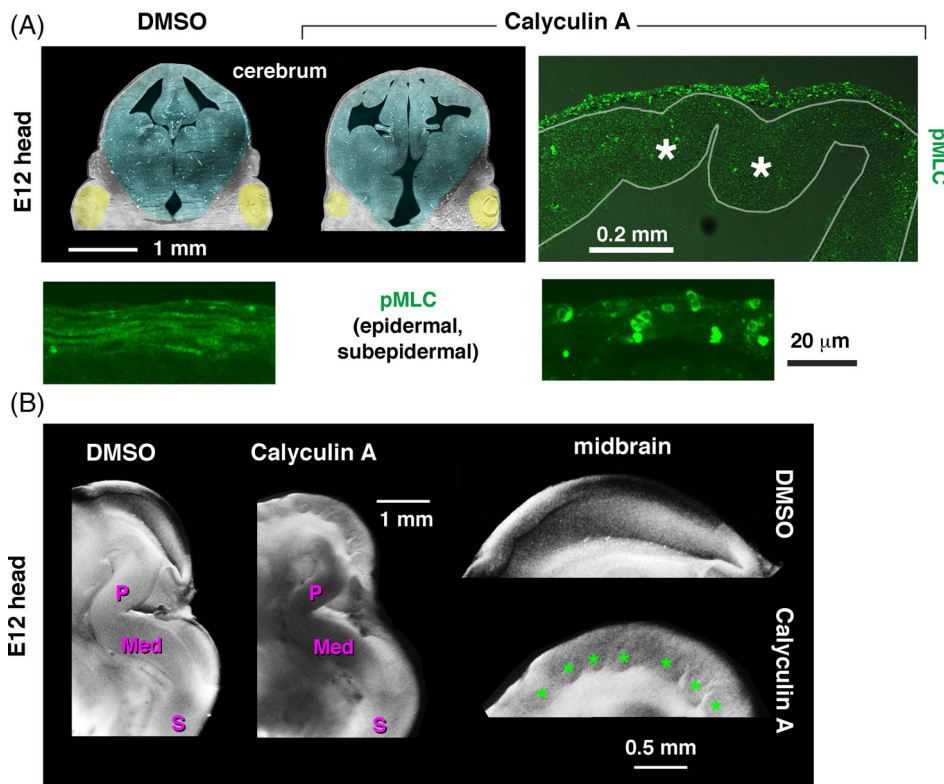


FIGURE 5 Calyculin A-induced contraction of the scalp in whole-head culture results in buckling of the E12 cerebral and midbrain walls. (A) Coronal sections of control (DMSO-treated) and calyculin A-treated E12 heads with high-magnification images of pMLC immunostaining. *abnormal convexity toward the lateral ventricle. (B) Sagittal sectional views of the right half of control and calyculin A-treated E12 heads. In the calyculin A-treated group, multiple buckled portions (*) were observed, and the angle between the pons (P) and the medulla (Med) appeared to be smaller. S, cervical spinal cord

$P = .03$ [Welch's test]) but not when the scalp was treated with collagenase ($59 \pm 11\%$ [$n = 9$], $P = .270$) (Figure 6A,B). In E12 embryos treated with elastase, a dorsal/outward displacement of the midbrain was observed ($n = 3/3$) (Figure 6C). This result suggests that elastin-mediated elasticity may also play a mechanical role in the embryonic scalp.

2.4 | Scalp removal affects brain morphology

We next asked whether the dorsal scalp, which is tangentially contractile and elastic, as shown above, truly contributes to the confinement of the brain, thereby causing stage-dependent morphological changes. We first focused on the degree of folding of the brainstem accompanied by the narrowing of the fourth ventricle (as shown in Figure 1). The angle between the pons and the medulla (P-Med angle) and the angle between the medulla and the cervical spinal cord (Med-S angle) were compared among scalp-intact heads, scalp-removed heads, and isolated brains at E13 (Figure 7A-C). The P-Med angle was

significantly greater in the scalp-removed heads ($76 \pm 6^\circ$ [$n = 7$], $P = 4.31 \times 10^{-5}$ [Welch's test]) and the isolated brains ($82 \pm 6^\circ$ [$n = 11$], $P = 1.61 \times 10^{-9}$) than in the scalp-intact (control) heads ($60 \pm 6^\circ$ [$n = 13$]), accompanied by the widening of the fourth ventricle along the rostrocaudal axis. This observation was consistent with the observation that the entire brain apparently showed a tendency for dorsal extrusion (similar to the phenomenon seen in an opened jack-in-the-box) in E13 heads in which the scalp was circularly incised to induce centripetal recoil (Figure 3). The Med-S angle was significantly greater in the scalp-removed heads ($89 \pm 5^\circ$ [$n = 7$], $P = .0048$) (but not in the isolated brain; $85 \pm 5^\circ$ [$n = 11$], $P = .0516$) than in the scalp-intact (control) heads ($81 \pm 6^\circ$ [$n = 10$]). Angle measurement was also performed in E13 heads treated with calyculin A (100 nM for 4 h or 1 μ M for 1 h). The P-Med angle was significantly smaller in the heads exposed to 100 nM calyculin A ($40 \pm 4^\circ$ [$n = 4$], $P = 8.40 \times 10^{-4}$ [Wilcoxon rank sum exact test]) and in those exposed to 1 μ M calyculin A ($53 \pm 1^\circ$ [$n = 4$], $P = 2.21 \times 10^{-3}$ [Welch's test]) than in the scalp-intact (control) heads ($60 \pm 6^\circ$ [$n = 13$]). The Med-S angle was also significantly smaller in the heads exposed to 100 nM calyculin A ($71 \pm 5^\circ$ [$n = 4$], $P = 2.67 \times 10^{-2}$ [Welch's test]) and those exposed to 1 μ M calyculin A ($71 \pm 3^\circ$ [$n = 4$], $P = 6.19 \times 10^{-3}$ [Welch's test]) than in the scalp-intact (control) heads ($81 \pm 6^\circ$ [$n = 4$]).

We next focused on the cerebrum. The maximal cerebral width (MCW) was significantly greater in vibratome slices prepared from scalp-removed heads (3.3 ± 0.1 mm [$n = 10$ sections from five heads], $P = 2.14 \times 10^{-3}$ [Welch's test]) than in those prepared from scalp-intact heads (3.0 ± 0.1 mm [$n = 12$ sections from six heads]) (Figure 7D,E). The area of the lateral ventricle (LV) (sum of bilateral measurements) was also significantly greater in vibratome sections prepared from scalp-removed heads (0.67 ± 0.24 mm² [$n = 10$ sections], $P = 2.88 \times 10^{-4}$ [Welch's test]) than in those prepared from scalp-intact heads (0.25 ± 0.12 mm² [$n = 12$ sections]) (Figure 7D,F). These differences inferred from the fixed scalp-intact and scalp-removed heads (Figure 7D-F) were directly confirmed by the continuous observation of freshly prepared live vibratome slices before and after scalp removal (Figure 7G): the MCW and the LV area became greater after the cerebral slices were freed from the scalp ($n = 3/3$).

2.5 | Scalp removal affects the distribution of cerebrospinal fluid

Since the mechanical homeostasis of embryonic cerebrospinal fluid (eCSF) influences the surface morphology of

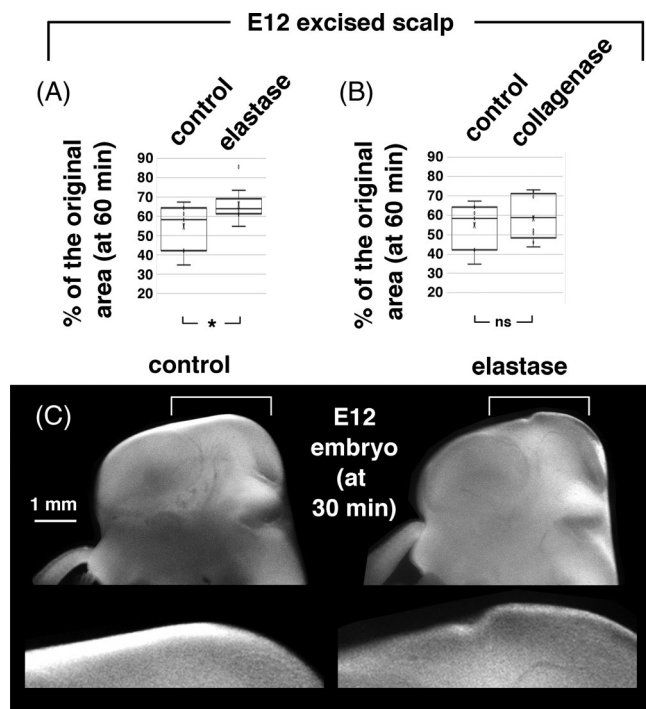


FIGURE 6 Assessment of the involvement of elastin and collagen in the recoil of the excised scalp. (A) Graph showing scalp shrinkage under treatment with elastase (2 U/mL, 60 min in total [30 min after excision]). * $P = .03$. (B) Graph showing scalp shrinkage under treatment with collagenase (2 mg/mL, 60 min in total [30 min after excision]). (C) Left-side views of control and elastase-treated E12 embryos with magnified views of the anterior midbrain region

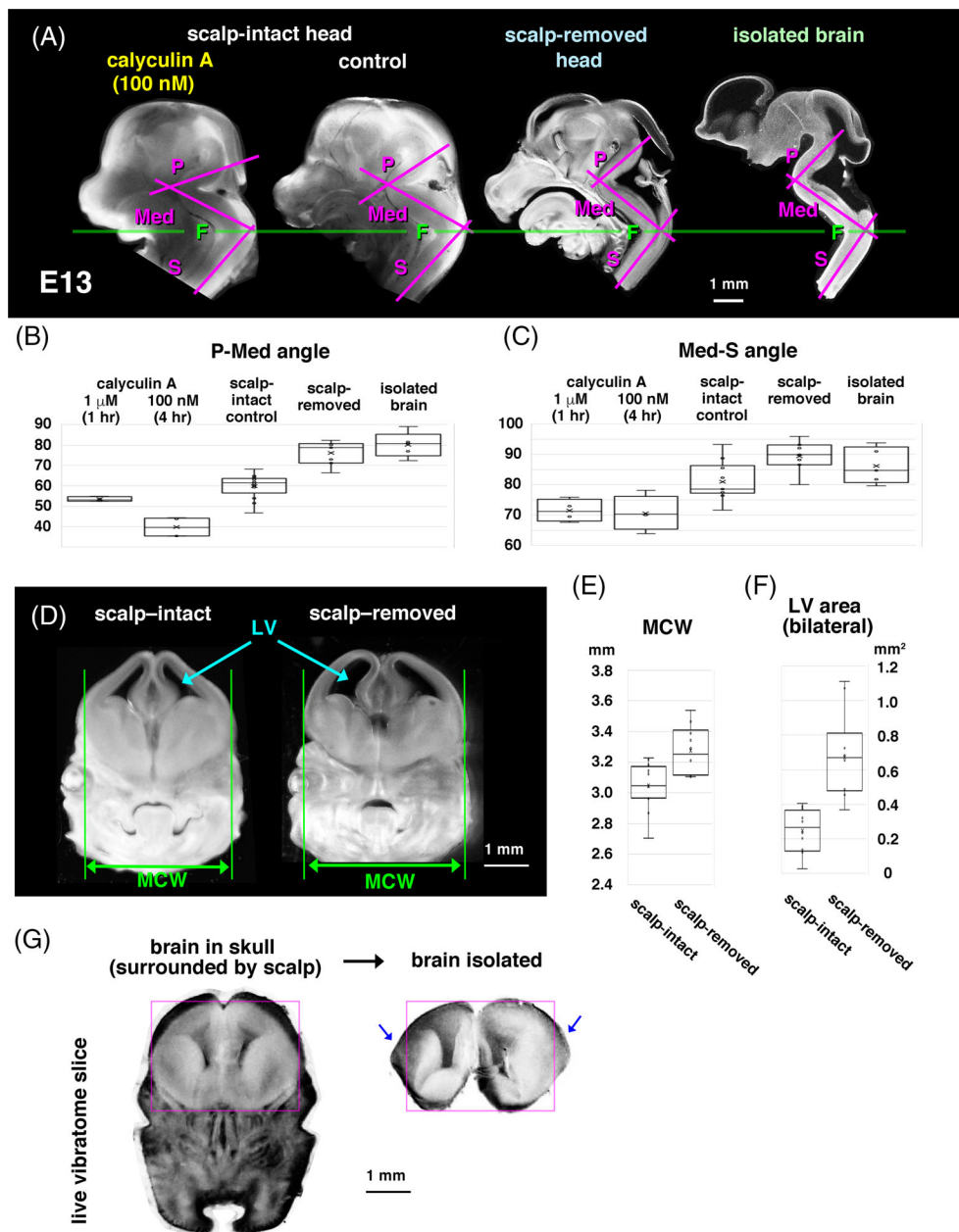


FIGURE 7 Effects of scalp removal on brain morphology at E13. (A) Sagittally sectioned right halves of a calyculin A-treated head (100 nM for 4 h), a scalp-intact (normal) head, a scalp-removed head, and an isolated brain. P, pons; Med, medulla; S, cervical spinal cord; F, cervical flexure.

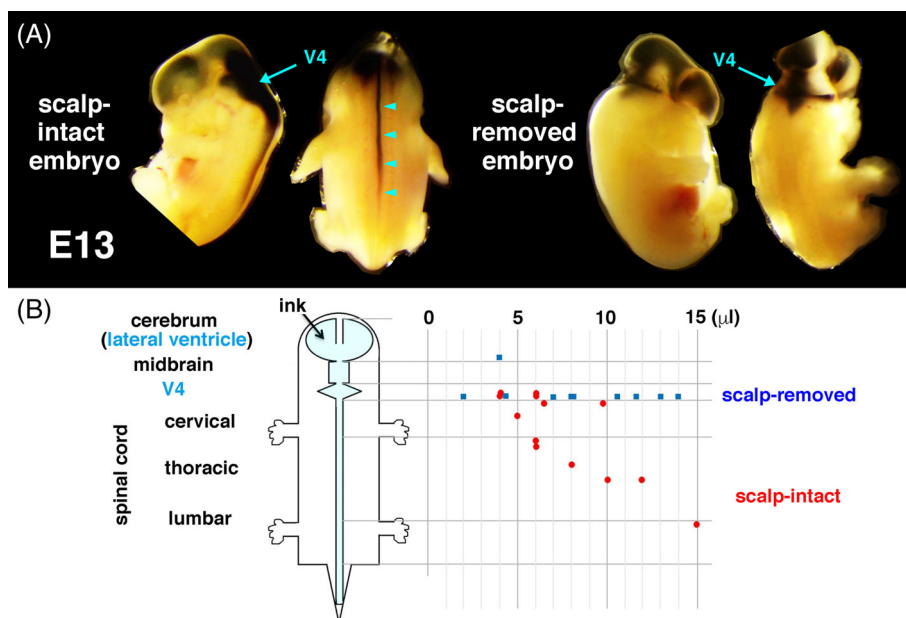
(B) Graph comparing the P-Med angle among the five groups (scalp-intact [untreated] heads, scalp-intact heads treated with 1 μ M calyculin A for 1 hour, scalp-intact heads treated with 100 nM calyculin A for 4 h, scalp-removed heads, and isolated brains). (C) Graph comparing the Med-S angle among the five groups.

(D) Coronal vibratome slices prepared from a fixed scalp-intact head and a fixed scalp-removed head at E13. LV, lateral ventricle; MCW, maximal cerebral width. (E) Graph comparing the MCW between the two (scalp-intact and scalp-removed) groups. (F) Graph comparing the LV area between the two groups. (G) Continuous live comparison of the morphology between an intracranial cerebral slice (left) and the same cerebral slice freed from the scalp (right). Widening (arrow) and LV enlargement were reproduced ($n = 3/3$)

the developing brain via outward pushing force,³⁵⁻³⁷ our discovery of scalp-imposed brain confinement prompted us to ask whether the contractile/elastic scalp might assist the brain in the distribution of eCSF. We focused specifically on eCSF delivery to the spinal cord, which has been speculated to occur under the influence of intracranial pressure.³⁸ While there are multiple eCSF-producing choroid plexus regions in the brain, the spinal cord lacks such regions. Inspired by the fact that the lower leg muscles contract and push the underlying veins to allow them to passively return blood to the heart,²⁹ we hypothesized that the E11–E13 scalp might play a constricting role similar to a leg muscle, contributing to

normal eCSF distribution via its compression activity. To test this hypothesis, we injected ink into the lateral ventricle in scalp-intact or scalp-removed embryos (Figure 8). In scalp-intact embryos, the ink easily spread caudally in a dose-dependent manner, entering the cervical spinal cord when a volume of approximately 5 μ L was administered and reaching more caudal levels when 10–15 μ L was administered. In contrast, ink injected into scalp-removed embryos remained in the brain, filling the ventricles in the brain to a great extent without entering the spinal cord (Figure 8A,B). These results suggest that the scalp may mechanically contribute to morphogenesis and eCSF homeostasis during brain development.

FIGURE 8 Effect of scalp removal on eCSF homeostasis at E13. (A) Normal and scalp-removed E13 embryos injected with ink in the lateral ventricle. V4, fourth ventricle. Arrowhead, ink dispersed into the spinal cord. (B) Graph showing the relationship between the volume of injected ink and the extent of ink spreading toward the caudal spinal cord in scalp-intact (red) and scalp-removed (blue) E13 embryos



Scalp cell proliferation decreases in brain-removed heads, while cells of excised scalps proliferate well when the tissue is restretched in culture.

Since physiological and clinically oriented skin expansion via cell proliferation is mediated by stretching,^{39,40} we next investigated whether the passive tangential stretching of the embryonic scalp, as is expected to occur during the mechanical confrontation of the scalp with the outwardly expanding brain in vivo (Figure 1), is associated with (or contributes to) normal proliferation in the scalp. To this end, we prepared two different 3D culture systems. First, normal and brain-removed E13 heads were cultured for 4 h, and bromodeoxyuridine (BrdU) was applied during the final 30 min. Low-power coronal section inspection revealed shrinkage of the scalp in the brain-removed heads (to 50% [on average, $n = 3$] of the size of the brain-intact scalp) (Figure 9A). Reflecting this tangential narrowing, the CX10⁺ epidermal layer was considerably thickened according to high-magnification views (Figure 9B). The total number of BrdU⁺ nuclei counted along the entire dorsal scalp length (between the bilateral eyelids) was significantly lower in the brain-removed group (54 ± 9 [$n = 3$], $P = .0013$ [Welch's test]) than in the normal group (104 ± 4 , $n = 3$) (Figure 9B,C), suggesting that cells that were in S phase of the cell cycle were significantly more abundant in the stretched epidermis of the brain-intact head than in the shrunken epidermis of the brain-removed head.

Second, we cultured excised scalp specimens under tensile (stretched) or zero-stress (released) conditions. This was necessary for the reliable assessment of the effect of stretching on proliferation in the healthy

nonepidermal (mesenchymal) layer because the oxygen supply to this relatively deep zone relative to the epidermis seemed insufficient under the first (whole-head culture) method. Another advantage of this second approach was that it allowed us to most clearly distinguish physical and chemical factors that, together, could have arisen from the brain under the first method. After the excised E13 scalp specimens shrank automatically (when released from the prestretched state), some were left in a recoiled state, and some were restretched using a device, as shown in Figure 9D (tightened with a silicone rubber ring to form a tympanum on a 2.5-mm-diameter drum). After 4 h of incubation (with BrdU exposure during the final 30 min), low-power inspection revealed healthy αSMA^+ mesenchymal layers in both groups. Under stretched culture, the αSMA^+ layer was thin, as observed in vivo, and the tangential length was up to 4–5 mm, including the 2.5-mm central tympanum area, while the αSMA^+ layer was only approximately 1.5–2 mm long and was much thicker under zero-stress culture than under stretched culture. The BrdU labeling (indicating normal entry into S phase) of the most distal part (originally most ventral, closest to the eyelid) appeared similar in the two types of explants. Within the central αSMA^+ layer, however, the BrdU labeling index was significantly lower in the zero-stress group ($6.2 \pm 4.7\%$ [$n = 4$], $P = .01$ [Welch's test]) than in the stretched group ($21.2 \pm 7.9\%$ [$n = 4$]). Similarly, the BrdU labeling index of the central epidermal (αSMA^-) layer was significantly smaller in the zero-stress group ($8.0 \pm 1.2\%$ [$n = 4$], $P = .002$) than in the stretched group ($17.9 \pm 3.1\%$ [$n = 4$]) (Figure 9E,F). Together, these results suggest that the tangential stretching of the scalp, as

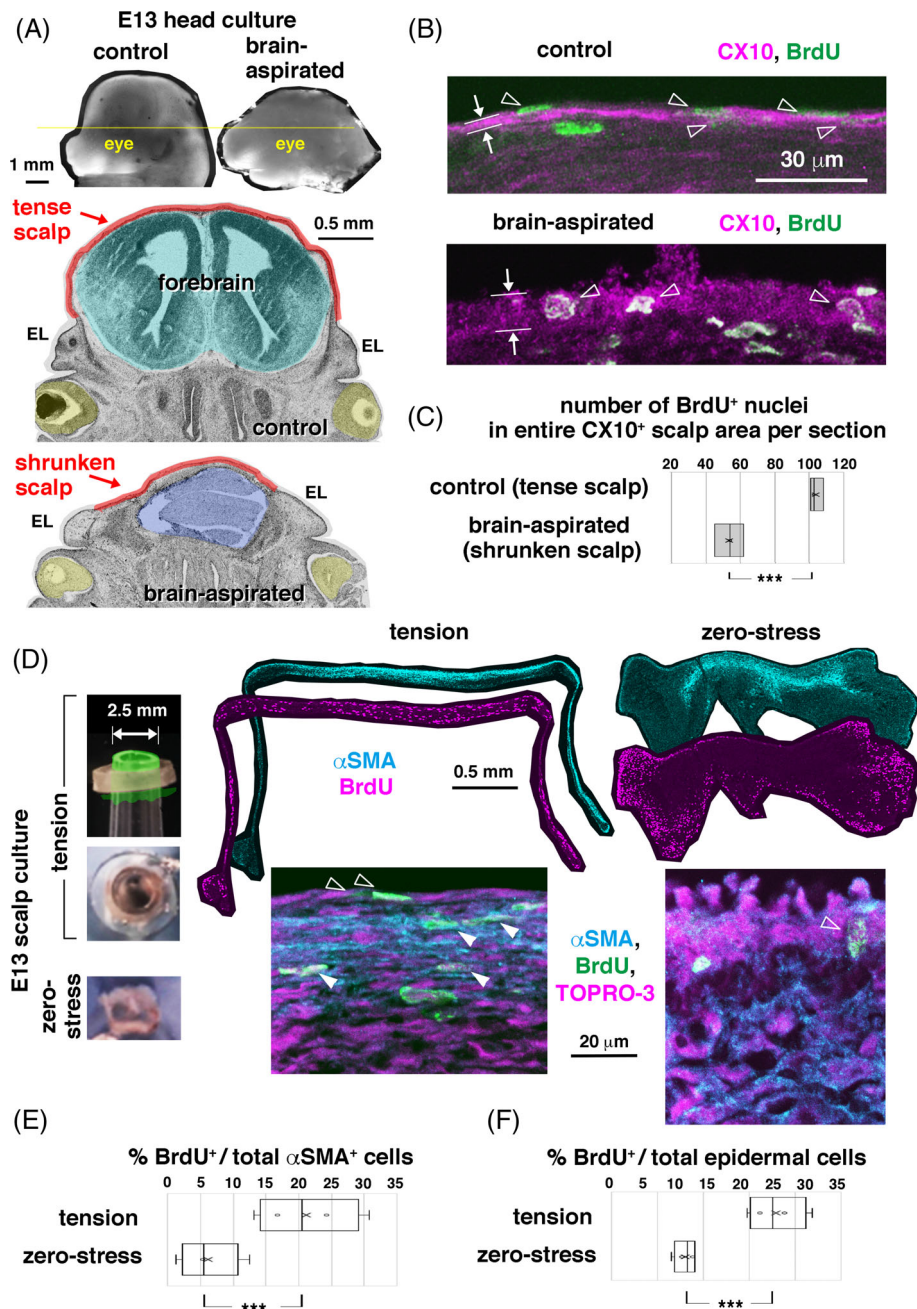


FIGURE 9 Assessment of the role of brain-mediated mechanical stretching on the proliferation of scalp cells. (A) Left-side views and coronal section views (at the level of the eye, highlighted in yellow) of normal and brain-removed E13 embryos cultured for 4 h, with bromodeoxyuridine (BrdU) addition during the final 30 min. EL, eyelid. (B) Magnified photomicrographs of the dorsal scalp immunostained with anti-CX10 and anti-BrdU. The epidermal layer (arrow) was thicker in the tangentially shrunken scalps of the brain-removed heads. (C) Graph comparing the total BrdU⁺ nuclei found in the CX10⁺ epidermal layer (open arrowhead) of the entire scalp area (defined as the area between the bilateral eyelids). (D) Circularly excised and shrunken E13 scalps were then cultured under restretched or zero-stress conditions for 4 h (with BrdU during the last 30 min) before cross-sectioning and immunostaining with anti- α SMA and anti-BrdU. A silicone rubber ring was used to tighten each stretched scalp (schematically shown in green in the side-view panel [upper], real image in the top-view panel [lower]) over the cut surface of a pipette tip. (E) Graph comparing the proportion of total α SMA⁺ cells (visualized with TOPRO-3) that were also positive for BrdU (solid arrowhead) between the two conditions. On average, 125 cells were counted in the tension culture group ($n = 4$), and 96 cells were counted in the zero-stress culture group ($n = 4$). (F) Graph comparing the proportion of total epidermal cells (most superficial, α SMA⁻) that were also positive for BrdU (open arrowhead) between the two conditions. On average, 32 cells were counted in the tension culture group ($n = 4$), and 73 cells were counted in the zero-stress culture ($n = 4$)

caused by outward pushing by the brain *in vivo*, may promote the proliferation of epidermal and mesenchymal cells at E13.

Measurement of the pressure needed to mechanically inflate/restretch the shrunken scalp.

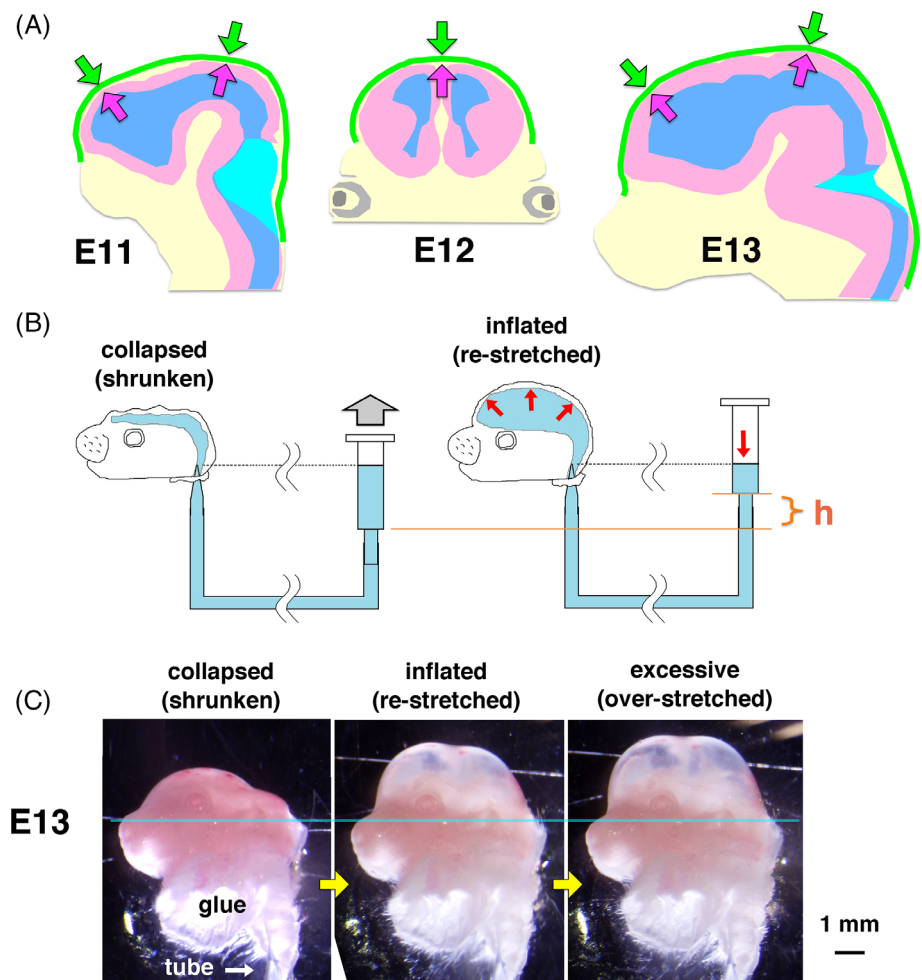
Finally, we sought to estimate the approximate level of pressure at which (a) outward pushing from the growing brain and (b) confinement of the brain by the scalp may exist in bidirectional balance (Figure 10A). To measure pressure in the context of this mechanical brain-scalp confrontation, we referred to a previously developed water manometer-based method⁴¹ and prepared a system to monitor pressures sufficient to fully inflate the shrunken scalp of the empty (brain-removed) head of an E13 embryo (Figure 10B,C). By lifting a medium-containing syringe connected to the embryo's collapsed head (Figure 10C, left panel), culture medium was introduced to the cranium. By measuring the height to which the syringe had to be lifted ("h" in Figure 10B, 8–12 mm) to achieve apparently sufficient ballooning of the scalp to restore the original contour (Figure 10C, middle panel), we estimated the pressure to be 77 ± 18 Pa ($n = 19$). This value was higher than the eCSF pressure measured at

E2–3 in chicks (15–30 Pa)^{37,41} and lower than the eCSF pressure at E19 in rats (147 Pa).⁴² Since our judgment as to whether the scalp was fully restretched to the same degree observed *in vivo* depended only on our monitoring of the contour of the scalp in lateral views, we assessed whether further pressurization might immediately result in excessive ballooning of the scalp. However, we found a lag until clear overballooning of the scalp was detected at 93 ± 16 Pa (Figure 10C, right panel). Therefore, the pressure at which mechanical confrontation between the growing brain and the scalp may occur in E13 mice *in vivo* is estimated to be between 77 and 93 Pa.

3 | DISCUSSION

The surgical removal of the scalp has long been no more than a preparative (brain-harvesting) step preceding the main experiments on the developmental mechanisms of the mammalian brain. However, surgical procedures such as slicing and incising brain tissues have been scientifically useful for elucidating mechanical events within the developing brain wall, such as passive cellular

FIGURE 10 Mechanical confrontation between the brain and the scalp and pressure measurements. (A) Schematic representation of sagittal sections of E11 and E13 heads and a coronal section of an E12 head. (B) Schematic illustration of a modified water manometer system applied to the brain-removed head of an E13 embryo for measuring the pressure needed to reballoon the collapsed/shrunken scalp. A syringe containing culture medium was connected through a flexible tube to the embryo's collapsed head. The original water surface (in the syringe) and the tip of the tube (in the embryo's collapsed cranium) were at the same level. When the syringe was lifted to a sufficient height (h), the culture medium introduced from the syringe through the tube inflated the cranium to balloon the scalp until it regained the original concavity. (C) An E13 head before and after inflation with medium. Blue line, drawn from the lower border of the eye to the ear



movements using a spring-like mechanism based on tissue elasticity,⁴³ the fencing of neural progenitor cells' moving somata by differentiating cells,⁴⁴ the expansion of the cerebral area via a landslide-like tissue spreading mechanism,⁴⁵ or abnormal delamination from the apical surface in response to overcrowding.¹³ In the present study, surgical treatments targeting the scalp (both epidermal and underlying mesenchymal layers) revealed remarkable and intriguing recoiling of the scalp in mice at E11-13 (Figure 3), a stage before the ossification of the skull. Circular incision-mediated centripetal scalp shrinkage continued until the scalp reached 52% of the original size (top view) by 20 min and 25% of its original size (3D view) by 40 min at E13 (Figure 3). The prestretch prerequisite for this cutting-induced recoiling of the scalp was found to depend on (a) optimized levels of actomyosin-mediated contraction in the epidermal and mesenchymal (preosteogenic) layers (Figures 2, 4 and 5); (b) elastin-associated extracellular matrix components distributed in these layers (Figures 2 and 6); and (c) outward pushing by the growing/expanding brain (at a pressure of approximately 77-93 Pa at E13) (Figures 3 and 10). The techniques used, the responses observed at the cellular and tissue levels, and the obtained measurements will be useful for further studies investigating the mechanisms underlying the development of the head, including the brain.

We showed that the confinement/compression of the brain by the scalp may underlie passive brainstem folding (narrowing of the angle between the pons and the medulla that occurs *in vivo* between E11 and E13) as well as the physiological morphogenesis of the cerebral hemispheres (Figure 7). This is in line with a previously proposed model indicating that regionally differential brain morphogenesis (while one region bulges or thickens toward the lumen, the neighboring region does not) can be partly explained by external mechanical factors.^{37,46} We also showed that the scalp may indirectly support eCSF homeostasis within the developing brain (Figure 8). Considering that the fluid-filled ventricle ensheathed with a thin brain wall is surrounded by contractile connective tissue, the embryonic scalp and the underlying brain vesicle can together be regarded as a hydrostatic skeleton system, as observed in the notochord^{47,48} and in invertebrate animals,⁴⁹ which would ensure the physical stiffness and morphological stability of the embryonic head during the period before calvarial ossification starts.

In addition to these scalp-to-brain physical contributions, the brain-mediated passive stretching of the scalp may underlie normal scalp cell proliferation (Figure 9), suggesting mechanical assistance from the brain to the scalp in turn. Brain-to-skull mechanical influences have been suggested to exist during the late (post-ossification)

period of head development.¹⁵ Stretch-induced proliferation has been established to occur in the adult or postnatal epidermis.⁴⁰ Thus, this study has widened our understanding of brain-to-scalp mechanical action, which has unexpectedly been shown to occur very early during head development. Importantly, this early embryonic brain-to-scalp load is coupled with scalp-to-brain influences. Thus, the brain and the scalp are in a close relationship whereby they mutually provide mechanical benefits to each other (Figures 1 and 10A). This scalp-brain mechanical interdependence or collaboration is reminiscent of a recently proposed model of engine-like positive feedback mediated by intertissue forces,^{50,51} although whether scalp-mediated confinement affects long-term brain-forming events such as proliferation or differentiation through mechanochemical coupling remains unknown and needs to be studied. It will also be important to study how the brain and meninges mechanically interact.¹⁵ In summary, we combined a variety of experimental methods to reveal that the early embryonic mouse brain and the surrounding scalp in the preosteogenic head elastically confront each other, building a stretcher-compressor relationship, and collaboratively developing in a mechanically interdependent manner.

4 | EXPERIMENTAL PROCEDURES

4.1 | Animals

The animal experiments were conducted according to the Japanese Act on Welfare and Management of Animals, the Guidelines for Proper Conduct of Animal Experiments (published by the Science Council of Japan), and the Fundamental Guidelines for Proper Conduct of Animal Experiments and Related Activities in Academic Research Institutions (published by the Ministry of Education, Culture, Sports, Science and Technology, Japan). All protocols for animal experiments were approved by the Animal Care and Use Committee of Nagoya University (No. 29006). Pregnant female mice (*Mus musculus*) were obtained from SLC (Hamamatsu, Japan; for ICR mice) or by mating at Nagoya University. Embryonic day (E) zero was defined as the day of vaginal plug identification.

4.2 | Immunofluorescence

Heads of embryonic mice (E11-E13) and cultured scalps were fixed with periodate-lysine-paraformaldehyde (PLP) fixative (containing 2% paraformaldehyde [PFA]) (4°C

1-3 h). For pMLC immunostaining, heads were fixed in PLP containing 2% trichloroacetic acid (1 h). After immersion in 20% sucrose, the heads were embedded in OCT compound (Miles), frozen and sectioned coronally (16 μ m). Cultured cells were fixed in 4% PFA for 15 min (room temperature). The frozen sections or fixed cells were treated with the following primary antibodies: anti-BrdU (rat, NB500-169; Novus Biologicals, 1:2000); anti- β III-tubulin (mouse, MMS-435P; Covance, 1:1000); anti-CD31/PECAM-1 (goat, AF3628, R&D, 1:300), anti-collagen 4 (rabbit, ab19808; Abcam, 1:500), anti-cytokeratin 10 (mouse, ab9025; Abcam, 1:500), anti-elastin (rabbit, ab21610; Abcam, 1:500), anti-pMLC (rabbit, ab2480; Abcam, 1:500), anti-Runx2 (rabbit, #12556; Cell Signaling, 1:1600), anti- α SMA (rabbit, 23 081-1-AP; Proteintech, 1:500), and anti-Tbx3 (rabbit, ab99302, Abcam, 1:300). After washing, the sections were treated with Alexa Fluor 488-, Alexa Fluor 546-, or Alexa Fluor 647-conjugated secondary antibodies (Molecular Probes, A-11029, A-11006, A-11034, A-11030, A-11035, A-11081, A-21236, A-21245, 1:200) and subjected to confocal microscopy (Olympus FV1000, Tokyo, Japan). In cultured cells, Alexa Fluor 546-conjugated phalloidin (A22283; Thermo Fisher Scientific, 1:1000) was used.

4.3 | Release of residual tissue stress

All surgical procedures conducted on embryos or heads were performed in culture medium (DMEM/F12) under a dissecting microscope (Leica MZ7.5 or MZ FLIII). Incisions in the scalps of E11 embryos were made using a microknife custom-made from a sewing-machine needle (Figure 3A). Scalps of E12 and older embryos were incised with microscissors (tip diameter 0.05 mm, cutting edge 3 mm; 15 000-00, Fine Science Tools). Care was taken not to damage the meninges and brain. To perform incisions in E13 embryos receiving placental circulation, a pregnant mother was anesthetized via the intraperitoneal administration of a mixture of 0.75 mg/kg medetomidine hydrochloride (Orion Pharma, ZENOAQ), 4 mg/kg midazolam (SANDZ), 5 mg/kg butorphanol tartrate (Meiji Seika), and 1.5 mg/kg atipamezole hydrochloride (Kyoritsu Seiyaku), and myometrium relaxation was induced by the intraperitoneal administration of 2 mg/kg ritodrine hydrochloride (FUJIFILM Wako). After midline laparotomy of the mother mouse, the uterine horn was pulled out and dipped into culture medium while the mother was kept on a stage positioned above the medium. Then, a small incision was made in the uterine wall and the amniotic sac to expose the embryo's head in medium. While surgical procedures were performed on the embryo's head (scalp), we monitored the heartbeat

and placental circulation. The aspiration of brain tissues from the cervical region was performed in culture medium using an aspiration device composed of a gel-loading tip (200 μ L, 010-Q, Quality Scientific Plastic) connected through a silicone tube to a suction pump (at 10-50 kPa, SP20, Markos Mefear). Since only a small portion of the brain could be dislodged and removed via a single aspiration, repetitive aspiration was necessary to remove the entire brain.

4.4 | Quantitative assessment of scalp shrinkage and brain angles

Heads or excised scalps were imaged using a system composed of either a dissecting microscope (Leica MZ7.5), an illuminator (SZ2-CLS, Olympus), and a CCD camera (SWIFTCAM, Swift Optical Instruments) or a dissecting microscope (Leica MZ FLIII), an illuminator (Hayashi LA150TA), and a CCD camera (ORCA ER, Hamamatsu Photonics). Top-view or cross-sectional analysis of the area of the scalp before or after shrinkage/recoil (Figures 3 and 4) was performed using ImageJ (National Institutes of Health, <https://imagej.nih.gov/ij/>). The measurement of scalp shrinkage through 3D reconstruction (Figure 3G) was performed after the circularly incised E13 heads were stained with 1% toluidine blue for 10-30 s (note: pretreatment with 1% Triton X-100 for 5 s facilitated staining). Approximately 48 images taken while the head was rotated and tilted were reconstructed using 3DF Zephyr (3Dflow, Verona, Italy). The area of the circularly disconnected scalp region (toluidine blue-stained and dorsally shrunken) and the entire area dorsal to the incision line (which represented almost the original scalp area) were compared.

4.5 | Pharmacological experiments

After incubating E12 heads for 30 min in culture medium containing only 0.5% DMSO (Sigma-Aldrich), 0.5% DMSO plus 20 μ M blebbistatin (Calbiochem), 0.5% DMSO plus 20 μ M Y27632 (Wako), 0.5% DMSO plus 2 mg/mL collagenase (Worthington), or 0.5% DMSO plus 2 U/mL elastase (Wako), a circular incision was made on each head. The excised scalps were further incubated under the same conditions for 30 min (total incubation time: 60 min). Cultured epidermal or mesenchymal cells were treated with culture medium containing only 0.1% DMSO (Sigma-Aldrich) or 0.1% DMSO plus 5 nM calyculin A (FUJIFILM Wako). For E12 or E13 heads, calyculin A was applied at 1 μ M for 60 min or 100 nM for 4 h.²³ Throughout the incubation of the heads or scalps,

the medium was carefully oxygenized with 95% O₂/5% CO₂ to prevent the intramembranous or perimeningeal vessels from contracting in response to hypoxia, as reported in embryonic mesenteric regions.⁵²

4.6 | Ink injection for evaluating the eCSF system

In each of the scalp-intact or scalp-removed E13 embryos, black ink (SHEAFFER Cartridge 96233, diluted 1:5 in phosphate-buffered saline) was injected into the lateral ventricle of a cerebral hemisphere using a glass capillary needle (created with a Narishige PN-30 tip puller) connected via a silicone rubber tube (1 mm diameter) to a PIPETMAN P200 pipette (GILSON).

4.7 | Assessment of scalp cell proliferation

Control and brain-removed E13 heads (Figure 9A) as well as shrunken and restretched scalps (Figure 9D) were incubated for 4 h in DMEM/F12 containing 5% horse serum (Gibco) and 5% fetal bovine serum (Gibco) in an incubator filled with 45% N₂, 40% O₂, and 5% CO₂ (APM-30D, Astec). Bromodeoxyuridine (BrdU) was added to the culture at 3.5 h, and the heads were fixed in 4% PFA at 4 h. For restretched culture (Figure 9D), each of the excised E13 scalps undergoing automatically shrinking (released from prestretched conditions in vivo) was placed onto the cut surface of a pipette tip (2.5 mm outer diameter) and tightened with a silicone rubber ring (made from a 1-mm-thick silicone rubber sheet [K-125, Togawa Rubber] using hollow punches [63395456, MonotaRO]). Parallel excised scalps that were not restretched were cultured under zero-stress (shrunken) conditions.

4.8 | Statistical analysis

The statistical analysis performed in this study compared the central tendencies of two populations based on samples of unrelated data. For this purpose, Welch's test was prioritized⁵³ on the basis of the normal sample distribution in each group. The Shapiro-Wilk normality test revealed that in most of the experimental groups of this study, the distribution was normal, and comparisons of the groups were accordingly conducted using Welch's test. In a few cases where distribution normality was not found, the Wilcoxon rank sum exact test was used.

4.9 | Pressure measurement using a water manometer

By modifying a previously developed water manometer system,⁴¹ we prepared a system to measure pressures sufficient for the full inflation of the scalp in the emptied (brain-removed) head of an E13 embryo (Figure 10B,C). Briefly, a gel-loading tip (200 µL, 010-Q, Quality Scientific Plastic), whose distal 25 mm was flexible, was inserted into the head with a glue seal at the neck and connected through a silicone rubber tube to a 1-mL syringe (Terumo). The syringe, containing DMEM/F12 (specific gravity 1.0168), was set with the tip facing down, and the plunger was removed. The level of the original water surface within the syringe and the level of the tip of the tube in the embryo's cranium were adjusted to be the same. The embryo's head was placed in a 60-mm culture dish containing DMEM/F12. Lifting of the syringe to a sufficient height (8–12 mm) sent culture medium into the cranium, expanding the scalp until it regained its original concavity (Figure 10C, middle) or showed overballooning (Figure 10C, right).

ACKNOWLEDGMENTS

We thank Takeo Matsumoto for valuable instructions about manometers; Reina Muramatsu, Namiko Noguchi, and Makoto Masaoka for excellent technical assistance; and members of Miyata laboratory for discussion.

AUTHOR CONTRIBUTIONS

Koichiro Tsujikawa: Conceptualization (lead); data curation (lead); formal analysis (lead); investigation (lead); methodology (lead); validation (lead); visualization (equal); writing – original draft (equal); writing – review and editing (equal). **Kanako Saito:** Conceptualization (equal); data curation (equal); formal analysis (equal); investigation (equal); methodology (equal); resources (equal); supervision (equal); validation (equal); visualization (equal); writing – original draft (equal); writing – review and editing (equal). **Arata Nagasaka:** Data curation (equal); investigation (equal); supervision (equal); validation (equal); writing – review and editing (equal).

ORCID

Takaki Miyata  <https://orcid.org/0000-0002-5952-0241>

REFERENCES

1. Goodwin K, Nelson CM. Mechanics of development. *Dev Cell*. 2021;56(2):240–250. doi:10.1016/j.devcel.2020.11.025
2. Weberling A, Zernicka-Goetz M. Trophectoderm mechanics direct epiblast shape upon embryo implantation. *Cell Rep*. 2021;34(3):108655. doi:10.1016/j.celrep.2020.108655

3. Hiramatsu R, Matsuoka T, Kimura-Yoshida C, et al. External mechanical cues trigger the establishment of the anterior-posterior axis in early mouse embryos. *Dev Cell*. 2013;27(2):131-144. doi:10.1016/j.devcel.2013.09.026
4. Savin T, Kurpios NA, Shye AE, et al. On the growth and form of the gut. *Nature*. 2011;476(7358):57-62. doi:10.1038/nature10277
5. Shyer A, Tallinen E, Nerurkar NL, et al. Villification: how the gut gets its villi. *Science*. 2013;342(6155):212-218. doi:10.1126/science.1238842
6. Kim HY, Pang M-F, Varner VD, et al. Localized smooth muscle differentiation is essential for epithelial bifurcation during branching morphogenesis of the mammalian lung. *Dev Cell*. 2015;34(6):719-726. doi:10.1016/j.devcel.2015.08.012
7. Varner VD, Gleghorn JP, Miller E, Radisky DC, Nelson CM. Mechanically patterning the embryonic airway epithelium. *Proc Natl Acad Sci U S A*. 2015;112(30):9230-9235. doi:10.1073/pnas.1504102112
8. Koyama H, Shi D, Suzuki M, Ueno N, Uemura T, Fujimori T. Mechanical regulation of three-dimensional epithelial fold pattern formation in the mouse oviduct. *Biophys J*. 2016;111(3):650-665. doi:10.1016/j.bpj.2016.06.032
9. Nelson CM. On buckling morphogenesis. *J Biomech Eng*. 2016;138(2):021005. doi:10.1115/1.4032128
10. Trushko A, Di Meglio I, Merzouki A, et al. Buckling of an epithelium growing under spherical confinement. *Dev Cell*. 2020;54(5):655-668. doi:10.1016/j.devcel.2020.07.019
11. Hosseini HS, Beebe DC, Taber L. Mechanical effects of the surface ectoderm on optic vesicle morphogenesis in the chick embryo. *J Biomech*. 2014;47(16):3837-3846. doi:10.1016/j.jbiomech.2014.10.018
12. Oltean A, Huang J, Beebe DC, Taber LA. Tissue growth constrained by extracellular matrix drives invagination during optic cup morphogenesis. *Biomech Model Mechanobiol*. 2016;15(6):1405-1421. doi:10.1007/s10237-016-0771-8
13. Okamoto M, Namba T, Shinoda T, et al. TAG-1-assisted progenitor elongation streamlines nuclear migration to optimize subapical crowding. *Nat Neurosci*. 2013;16(11):1556-1566. doi:10.1038/nn.3525
14. Koser DE, Thompson AJ, Foster SK, et al. Mechanosensing is critical for axon growth in the developing brain. *Nat Neurosci*. 2016;19(12):1592-1598. doi:10.1038/nn.439415
15. Richtsmeier JT, Flaherty K. Hand in glove: brain and skull in development and dysmorphogenesis. *Acta Neuropathol*. 2013;125(4):469-489. doi:10.1007/s00401-013-1104-y
16. Clark WELG. Deformation patterns in the cerebral cortex. In: Le Gross Clark WE, Medawar PB, eds. *Essays on Growth and Form*. London, UK: Oxford University Press; 1945:1-22.
17. Barron DH. An experimental analysis of some factors involved in the development of the fissure pattern of the cerebral cortex. *J Exp Zool*. 1950;113:553-581. doi:10.1002/jez.1401130304
18. Richman DP, Stewart RM, Hutchinson JW, Caviness VS Jr. Mechanical model of brain convolutional development. *Science*. 1975;189(4196):18-21. doi:10.1126/science.1135626
19. Tallinen T, Chung J, Rousseau F, et al. On the growth and form of cortical convolutions. *Nature Phys*. 2016;12:588-593. doi:10.1038/nphys363220
20. Pikalow AS, Flynn ME, Searls RL. Development of cranial flexure and Rathke's pouch in the chick embryo. *Anat Rec*. 1994;238(3):407-414. doi:10.1002/ar.1092380315
21. Takamatsu T, Fujita S. Growth of notochord and formation of cranial and mesencephalic flexures in chicken embryo. *Develop Growth and Differ*. 1987;29(5):497-502. doi:10.1111/j.1440-169X.1987.00497.x
22. Garcia KE, Okamoto RJ, Bayly PV, Taber LA. Contraction and stress-dependent growth shape the forebrain of the early chicken embryo. *J Mech Behav Biomed Mater*. 2017;65:383-397. doi:10.1016/j.jmbbm.2016.08.010
23. Filas BA, Oltean A, Majidi S, Bayly PV, Beebe DC, Taber LA. Regional differences in actomyosin contraction shape the primary vesicles in the embryonic chicken brain. *Phys Biol*. 2012;9(6):066007. doi:10.1088/1478-3975/9/6/066007.16
24. Morris-Kay GM. Derivation of the mammalian skull vault. *J Anat*. 2001;199(pt1-2):143-151. doi:10.1046/j.1469-7580.2001.19910143.x
25. Rice R, Rice DPC, Olsen BR, Thesleff I. Progression of calvarial bone development requires Foxc1 regulation of *Msx2* and *Alx4*. *Dev Biol*. 2003;262(1):75-87. doi:10.1016/s0012-1606(03)00355-5
26. Roybal PG, Wu NL, Sun J, Ting MC, Schafer CA, Maxson RE. Inactivation of *Msx1* and *Msx2* in neural crest reveals an unexpected role in suppressing heterotopic bone formation in the head. *Dev Biol*. 2010;343(1-2):28-39. doi:10.1016/j.ydbio.2010.04.007
27. Cesario JM, Landin Malt A, Chung JU, et al. Anti-osteogenic function of a LIM-homeodomain transcription factor LMX1B is essential to early patterning of the calvaria. *Dev Biol*. 2018;443(2):103-116. doi:10.1016/j.ydbio.2018.05.022
28. Lee C, Richtsmeier JT, Kraft RH. A coupled reaction-diffusion-strain model predicts cranial vault formation in development and disease. *Biomech Model Mechanobiol*. 2019;18(4):1197-1211. doi:10.1007/s10237-019-01139-z
29. Calnan JS, Pflug JJ, Mills CJ. Pneumatic intermittent-compression legging simulating calf-muscle pump. *Lancet*. 1970;296(7671):502-503. doi:10.1016/s0140-6736(70)90118-2
30. Miyai Y, Esaki N, Takahashi M, Enomoto A. Cancer-associated fibroblasts that restrain cancer progression: hypotheses and perspectives. *Cancer Sci*. 2019;111(4):1047-1057. doi:10.1111/cas.14346
31. Hadden M, Mittal A, Samra J, Zreiqat H, Sahni S, Ramaswamy Y. Mechanically stressed cancer microenvironment: role in pancreatic cancer progression. *Biochim Biophys Acta Rev Cancer*. 2020;1874(2):188418. doi:10.1016/j.bbcan.2020.188418
32. Abzhanov A, Rodda SJ, McMahon AP, et al. Regulation of skeletogenic differentiation in cranial dermal bone. *Development*. 2007;134(17):3133-3144. doi:10.1242/dev.002709
33. Suzuki A, Itoh T. Effects of calyculin A on tension and myosin phosphorylation in skinned smooth muscle of the rabbit mesenteric artery. *Br J Pharmacol*. 1993;109(3):703-712. doi:10.1111/j.1476-5381.1993.tb13631.x
34. Sugita S, Mizutani E, Hozaki M, Nakamura M, Matsumoto T. Photoelasticity-based evaluation of cellular contractile force for phenotypic discrimination of vascular smooth muscle cells. *Sci Rep*. 2019;9(1):3960. doi:10.1038/s41598-019-40578-7
35. Pexieder T, Jelinek R. Pressure of the CSF and the morphogenesis of CNS. II. Pressure necessary for normal development of brain vesicle. *Physiol Bohemoslov*. 1970;18(2):181-192.
36. Desmond ME, Jacobson AG. Embryonic brain enlargement requires cerebrospinal fluid pressure. *Dev Biol*. 1977;57(1):188-198. doi:10.1016/0012-1606(77)90364-5
37. Garcia KE, Stewart WG, Espinosa MG, Gleghorn JP, Taber LA. Molecular and mechanical signals determine morphogenesis

- of the cerebral hemispheres in the chicken embryo. *Development*. 2019;146(20):dev174318. doi:10.1242/dev.174318
38. Akai T, Hatta T, Shimada H, et al. Extracranial outflow of particles solved in cerebrospinal fluid: fluorescein injection study. *Congenit Anom*. 2018;58(3):93-98. doi:10.1111/cga.12257
39. Zöllner AM, Holland MA, Honda KS, Gosain AK, Kuhl E. Growth on demand: reviewing the mechanobiology of stretched skin. *J Mech Behav Biomed Mater*. 2013;28:495-509. doi:10.1016/j.jmbbm.2013.03.018
40. Aragona M, Sifrim A, Malfait M, et al. Mechanisms of stretch-mediated skin expansion at single-cell resolution. *Nature*. 2020;584(7820):268-273. doi:10.1038/s41586-020-2555-7
41. Jelinek R, Pexieder T. The pressure of encephalic fluid in chick embryos between the 2nd and 6th day of incubation. *Physiol Bohemoslov*. 1968;17(3):297-305.
42. Jones HC, Bucknall RM. Changes in cerebrospinal fluid pressure and outflow from the lateral ventricles during development of congenital hydrocephalus in the H-Tx rat. *Exp Neurol*. 1987;98(3):573-383. doi:10.1016/0014-4886(87)90266-4
43. Shinoda T, Nagasaka A, Inoue Y, et al. Elasticity-based boosting of neuroepithelial nucleokinesis via indirect energy transfer from mother to daughter. *PLoS Biol*. 2018;16(4):e2004426. doi:10.1371/journal.pbio.2004426
44. Watanabe Y, Kawaue T, Miyata T. Differentiating cells mechanically limit the interkinetic nuclear migration of progenitor cells to secure apical cytotogenesis. *Development*. 2018;145(14):dev162883. doi:10.1242/dev.162883
45. Saito K, Okamoto M, Watanabe Y, et al. Dorsal-to-ventral cortical expansion is physically primed by ventral streaming of early embryonic preplate neurons. *Cell Rep*. 2019;29(6):1555-1567. doi:10.1016/j.celrep.2019.09.075
46. Nagasaka A, Miyata T. Comparison of the mechanical properties between the convex and concave inner/apical surfaces of the developing cerebrum *front cell*. *Dev Biol*. 2021;9:702068. doi:10.3389/fcell.2021.702068
47. Adams DS, Keller R, Koehl MAR. The mechanics of notochord elongation, straightening and stiffening in the embryo of *Xenopus laevis*. *Development*. 1990;110(1):115-130.
48. Jiang D, Smith WC. Acidian notochord morphogenesis. *Dev Dyn*. 2007;236(7):1749-1757. doi:10.1002/dvdy.21184
49. Kier WM. The diversity of hydrostatic skeletons. *J Exp Biol*. 2012;215:1247-1257. doi:10.1242/jeb.056549
50. Xiong F, Ma W, Bénazéraf B, Mahadevan L, Pourquié O. Mechanical coupling coordinates the co-elongation of axial and paraxial tissues in avian embryos. *Dev Cell*. 2020;55(3):354-366. doi:10.1016/j.devcel.2020.08.007
51. Trubuil É, Solon J. A compression engine to coordinate tissue elongation in the embryo. *Dev Cell*. 2020;55(3):256-258. doi:10.1016/j.devcel.2020.10.013
52. Brinks L, Moone RM, Moral-Sanz J, et al. Hypoxia-induced contraction of chicken embryo mesenteric arteries: mechanisms and developmental changes. *Am J Physiol Regul Integr Com Physiol*. 2016;311(5):R858-R869. doi:10.1152/ajpregu.00461.2015
53. Ruxton GD. The unequal variance *t*-test is an underused alternative to Student's *t*-test and the Mann-Whitney *U* test. *Behavior Ecol*. 2006;17:688-690. doi:10.1093/beheco/ark016

SUPPORTING INFORMATION

Additional supporting information may be found in the online version of the article at the publisher's website.

How to cite this article: Tsujikawa K, Saito K, Nagasaka A, Miyata T. Developmentally interdependent stretcher-compressor relationship between the embryonic brain and the surrounding scalp in the preosteogenic head. *Developmental Dynamics*. 2022;251(7):1107-1122. doi:10.1002/dvdy.451